Building and Environment 205 (2021) 108272

Contents lists available at ScienceDirect

Building and Environment

journal homepage: www.elsevier.com/locate/buildenv

Model predictive control for energy-efficient optimization of radiant ceiling cooling systems

Qiong Chen, Nan Li *

National Centre for International Research of Low-carbon and Green Buildings, Ministry of Science & Technology, Chongqing University, Chongqing, 400045, China

ARTICLE INFO

Keywords:
Model predictive control (MPC)
Radiant ceiling cooling
Energy efficiency
Model order reduction
Robustness

ABSTRACT

State-of-the-art model predictive control (MPC) applications have been performed in various heating and cooling systems of buildings, such as fan coil unit systems and radiant floor heating systems. However, there is also a significant potential for improved zone air temperature control for better thermal comfort and efficient energy savings in increasingly prosperous radiant ceiling cooling systems. In this research, the physics-based model was developed by applying the building envelope configuration and material property information. The reduced-order model of the original radiant ceiling cooling system model was then simplified using the balanced truncation method for reducing computational cost and maintaining a comparative model accuracy. The model predictive control of radiant ceiling cooling systems was proposed for zone air temperature tracking, allowing the system to be more robust and adaptive to external thermal disturbances such as solar radiation and ambient temperature. The superior performance of model predictive control in terms of accurate zone air temperature tracking and energy efficiency was evaluated by a simulation compared to PID control and conventional bang-bang control in both continuous and intermittent operation. The proposed model predictive control can achieve 21%–27% and 6% energy saving efficiency, compared with PID control and conventional bang-bang control, respectively. And there is rarely any overshoot or steady-state error presence for the zone air temperature, which demonstrated the significant potential of the robust model predictive control for better thermal comfort and efficient energy savings in growing prosperous radiant ceiling cooling systems.

1. Introduction

As one of the three major energy consumption and carbon emissions areas along with industries and transportation, buildings account for about 1/3rd of China's total energy consumption and about 70% in other countries of the world such as the United States where building heating, ventilation, and air conditioning systems (HVAC system) account for a significant portion of a building's energy consumption [1,2]. Therefore, the energy-efficient operation of building HVAC systems is extraordinarily significant for promoting energy efficiency and carbon neutrality in the building sector and society as a whole [3]. Radiant cooling systems [4] have a great potential for energy-efficient operations because they have the advantage of being coupled with low-temperature heat sources, such as air energy and other renewable energy sources, to increase the water supply temperature of the cooling system. This, in turn, contributes to the performance enhancement of system chillers [5].

Therefore, there is a lot of research literature related to the evaluation of performance indicators and control strategy [6,7] optimization for radiant cooling systems. Jingjuan (Dove) FENG et al. [8] summarized the design approach for radiant cooling systems and identified potential gaps and limitations in design practice through 12 surveys, eight interviews with key practitioners, and a literature review. The chilled water temperature control of radiant cooling systems should not only meet the requirements of a comfortable indoor thermal environment but should also pay attention to anti-condensation on the radiant surface. In the literature, Muhammed A. Hassan [9] has stated in the literature that adjusting the chilled water temperature or flow rate was usually considered as one of the various methods to achieve an optimal control operation of the system. However, it was much more reliable to control the radiant surface temperature or the average water temperature in practical applications. A model predictive control (MPC) based intelligent operation strategy was proposed by Jaewan Joe [10] to optimize the performance of hydronic radiant floor systems in office buildings by dynamically estimating the zone loads, and temperatures, and minimizing the energy consumption and costs while meeting the equipment and thermal comfort requirements. The research results

* Corresponding author.
E-mail address: nanlicqu@163.com (N. Li).

https://doi.org/10.1016/j.buildenv.2021.108272
Received 31 May 2021; Received in revised form 13 August 2021; Accepted 17 August 2021
Available online 19 August 2021

Nomenclature

$\widetilde{C}_{air}$	The heat capacity matrix of the zone air
$\widetilde{C}_c$	The heat capacity matrix of the radiant ceiling
$\widetilde{C}_w$	The heat capacity matrix of the building envelopes
H_z	The conductive heat transfer coefficient matrix of the radiant ceiling
H_{zc}	The radiant heat transfer coefficient matrix of the radiant ceiling
H_{zw}	The convective heat transfer coefficient matrix of the radiant ceiling
H_w	The conductive heat transfer coefficient matrix of the building envelopes
H_{wc}	The radiant heat transfer coefficient matrix of the building envelopes
H_{wz}	The convective heat transfer coefficient matrix of the building envelopes
λ	Thermal conductivity, W/m·K
c	The specific heat capacity of the envelope layers, J/(kg·°C)
R_x	The conductive thermal resistance of the core layer in the radiant ceiling, m^2·K/W
R_w	The convective thermal resistor on the internal buried pipe surface, m^2·K/W
R_r	The conductive thermal resistor of the buried pipe, m^2·K/W
R_x	The conductive thermal resistor of the core layer of the radiant ceiling, m^2·K/W
T_c	The vector of temperature nodes of the radiant ceiling, °C
T_w	The vector of temperature nodes of the building envelope, °C
T_z	The vector of temperature nodes of the zone air, °C
q_c	The heat flow matrix for the radiant ceiling
q_w	The heat flow matrix for the building envelopes
q_z	The heat flow matrix for the zone air
W_c	The controllability Gram matrix
W_o	The observable Gram matrix
Γ	The Hankel matrix

showed a 34% cost savings for the MPC over a baseline feedback control during the cooling season. The thermal response index, namely the heat storage efficiency (HSE), of radiant cooling systems was tested by Michal Krajcíd et al. [11] Cooling systems with different combinations of tube locations, material layer structures, and heat core materials were compared. In addition, a new thermal output index (ETO), i.e., an effective thermal output, was proposed which considered both the steady-state thermal characteristics represented by the nominal heat output and the dynamic thermal characteristics represented by the thermal storage efficiency. Xiufeng Pang et al. [12] showed that a simplified MPC approach applied to radiant panel cooling systems can achieve more energy savings than conventional control strategies [13]. This can be done through field experiments, yielding 42% chilled water pump power and 16% cooling energy savings, while guaranteeing equal or better indoor comfort.

Despite the excellent energy-saving potential of radiant cooling systems [14], the control of current cooling systems may not take full advantage of the low temperature heat sources [15], especially when the building cooling load and outdoor environmental parameters change dynamically [16]. In addition to this, the energy-saving potential of the system under variable water temperature control is supposed to be fully explored to improve the adaptability to the outdoor thermal environment as well. This means that the water temperature can be increased to achieve an energy efficient operation of the system when the radiant ceiling cooling system is carried with a lower cooling load [17]. The objective of this study is to develop an MPC [18] for radiant ceiling cooling systems to improve the system's adaptation to the environment and to evaluate the energy saving potential of the MPC using simulation methods.

Extensive research has been conducted for decades on the application of MPC in the architecture field [19–21]. Ján Drgoňa [22] demonstrated the excellent performance of the MPC through the actual operating results of a ground source heat pump (GSHP) system [23] that yielded significant energy savings of 53.5% of energy use and 36.9% improvement in thermal comfort during the most unfavorable seasons. Jian Fang et al. [24] proposed an MPC-based optimal control strategy for different application scenarios and defined the conversion efficiency as the ratio between PMV change and energy consumption reduction, resulting in an efficiency improvement of 29.2%–49.8%. Furthermore, the optimal control of a plate heat exchanger using MPC was investigated through a large-scale case study. The experimental results showed that the control response of the system can be improved and the energy consumption can be reduced by introducing soft constraints in the MPC design [25]. An experimental and numerical study of model predictive control of hybrid ventilation [26] was performed in an institutional building, focusing on improving thermal comfort. The experimental results demonstrated that the proposed control strategy can increase the energy-saving potential by a factor of five at the expense of thermal comfort [27].

Shiyu Yang et al. [28] found that the MPC control achieved energy savings of 14.7% and 20% for conventional fan coil unit systems and active chilled beam systems, respectively, while keeping the indoor thermal comfort within acceptable limits. This demonstrated that the application of MPC controllers can effectively improve the energy efficiency of ACMV systems (air conditioning mechanical ventilation systems). Sophie Yuan et al. [29] evaluated the energy-saving performance of applying the MPC to a hybrid ventilation system for buildings with high thermal capacity. Using the humidity ratio instead of relative humidity as a criterion for evaluating outdoor air can extend the effective use of the system by 49%–180% within one year. Dongliang Zhang et al. [30] evaluated the energy-saving potential of the RFCUV (radiant floor cooling combined with the underfloor ventilation) system. The MPC controller achieved 17.5% energy savings while maintaining equal or better indoor comfort. Besides, MPC showed the advantages of a fast response, excellent stability, and efficient energy savings compared to PID for RFCUV systems. Moreover, they also evaluated the energy-saving potential of the MPC applied to the RCCUV (radiant ceiling cooling integrated with the underfloor ventilation) system in Nanjing. The MPC controller reduced the energy consumption of the RCCUV system by 13.2%, compared to the PID (proportion integral differential) controller during the 2-h experimental period, confirming that the optimal performance of the MPC is superior to the PID control [31]. Mohammad M. Mazar [32] applied the MPC to minimize the energy consumption during the boiler's start-up time, using a building model combined with weather forecast data to operate the actuator in the best possible way while staying within the thermal comfort limits. A comparative analysis with conventional control methods showed that the proposed MPC saved 13% energy during the boiler's start-up time.

Besides, various research on the MPC has been carried out in the field of the large-scale PV plant [33], integration of zone air temperature integrated with humidity control [34,35], hybrid geothermal systems [36], space heating systems [37], etc. The current research on MPC optimization has focused on the conventional building heating or cooling system [38,39], such as fan coil unit systems [40,41] and radiant

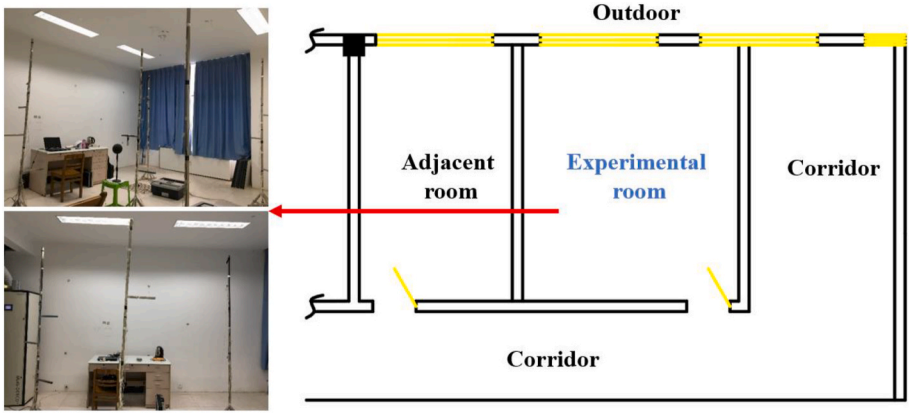

Fig. 1. The schematic diagram of the experimental cell for the radiant ceiling cooling system.

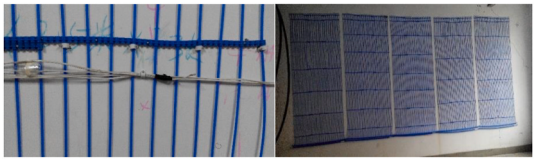

Fig. 2. Schematics of the capillary-mat radiant ceiling in the experimental cell.

floor heating systems [42], while few studies have been conducted to evaluate the energy-saving potential of ceiling radiant cooling systems. At present, the comprehensive research on a state-of-the-art MPC applied to radiant ceiling cooling systems should be fully developed to facilitate the application of this system more and more widely in the future.

Section 2 introduces the model formulation of the radiant ceiling cooling system based on the physical properties of building envelope materials and geometric dimensions where the developed model's accuracy was validated through the comparative analysis of the experiment and simulation results. The model order reduction based on the balanced truncation method is carried out for the simplification of the higher-order model of the radiant ceiling cooling system in Section 3. Then the MPC framework, as illustrated in Section 4, aims at improving the energy efficiency, the dynamic response performance as well as the PID control, and the conventional bang-bang control while taking the external thermal disturbances such as solar radiation and ambient temperature as predictable parameters. The simulation results indicating the dynamic response performance and energy-saving potential under continuous and intermittent operations are exhibited in Section 5. Finally, the conclusions of the evaluation of MPC applications available for radiant ceiling cooling systems are provided in Section 6.

2. Building model development

2.1. State-space representation of the radiant ceiling cooling system

The experimental cell for the radiant ceiling cooling system is located on the fourth floor of the experimental building of Chongqing University, with geometric dimensions of 6 m × 5 m × 3.2 m (lenghth × width × height), respectively. The schematic diagram of the experimental cell for the radiant ceiling cooling system is shown in Fig. 1. The schematics of the capillary-mat radiant ceiling in the experimental cell are presented in Fig. 2. The capillary mats have geometrical dimensions of 1000 mm x 10,000 mm and a total laying area of 20 m^2 on the radiant ceiling, and each capillary mat is laid in a folded form. The average daily ambient temperature is 32.4°*C*–35.1°*C* with the highest temperature reaching about 41.5°*C* during the experimental period.

A heat transfer model of the radiant ceiling cooling system is first required before establishing an MPC. In this study, a state-space model based on physical property parameters is used which has achieved good accuracy and excellent applications in previous studies, is used [1,43]. A radiant ceiling containing an embedded heat source needs to be characterized by a three-dimensional heat transfer process including heat transfer along the direction of the water flow in the pipe, convective heat transfer on the inner surface of the pipe wall, the thermal conductivity of the pipe wall, and thermal conductivity of the core temperature layer. The heat transfer equations of the building envelopes such as exterior walls, interior walls, and floor slabs, the complicated radiant ceiling [44], and the zone air are listed in Eq. (1)–(3), respectively, and the state-space representation of the radiant ceiling cooling system presented in Eq. (4) can be obtained by combining the above heat transfer equations.

$$\widetilde{C}_c \dot{\overrightarrow{T}}_c = \widetilde{H}_c \overrightarrow{T}_c + \widetilde{H}_{cw} \overrightarrow{T}_w + \widetilde{H}_{cz} \overrightarrow{T}_z + \overrightarrow{q}_c \tag{1}$$

$$\widetilde{C}_w \dot{\overrightarrow{T}}_w = \widetilde{H}_{wc} \overrightarrow{T}_c + \widetilde{H}_w \overrightarrow{T}_w + \widetilde{H}_{wz} \overrightarrow{T}_z + \overrightarrow{q}_w \tag{2}$$

$$\widetilde{C}_{air} \dot{\overrightarrow{T}}_z = \widetilde{H}_{zc} \overrightarrow{T}_c + \widetilde{H}_{zw} \overrightarrow{T}_w + \widetilde{H}_z \overrightarrow{T}_z + \overrightarrow{q}_z \tag{3}$$

$$\begin{aligned}
\begin{bmatrix} \dot{\overrightarrow{T}}_c \\ \dot{\overrightarrow{T}}_w \\ \dot{\overrightarrow{T}}_z \end{bmatrix} &= \begin{bmatrix} \widetilde{C}_c & 0 & 0 \\ 0 & \widetilde{C}_w & 0 \\ 0 & 0 & \widetilde{C}_{air} \end{bmatrix}^{-1} \begin{bmatrix} \widetilde{H}_c & \widetilde{H}_{cw} & \widetilde{H}_{cz} \\ \widetilde{H}_{wc} & \widetilde{H}_w & \widetilde{H}_{wz} \\ \widetilde{H}_{zc} & \widetilde{H}_{zw} & \widetilde{H}_z \end{bmatrix} \begin{bmatrix} \overrightarrow{T}_c \\ \overrightarrow{T}_w \\ \overrightarrow{T}_z \end{bmatrix} \\
&+ \begin{bmatrix} \widetilde{C}_c & 0 & 0 \\ 0 & \widetilde{C}_w & 0 \\ 0 & 0 & \widetilde{C}_{air} \end{bmatrix}^{-1} \begin{bmatrix} \overrightarrow{q}_c \\ \overrightarrow{q}_w \\ \overrightarrow{q}_z \end{bmatrix} \\
&= \begin{bmatrix} \widetilde{C}_c & 0 & 0 \\ 0 & \widetilde{C}_w & 0 \\ 0 & 0 & \widetilde{C}_{air} \end{bmatrix}^{-1} \begin{bmatrix} \widetilde{H}_c & \widetilde{H}_{cw} & \widetilde{H}_{cz} \\ \widetilde{H}_{wc} & \widetilde{H}_w & \widetilde{H}_{wz} \\ \widetilde{H}_{zc} & \widetilde{H}_{zw} & \widetilde{H}_z \end{bmatrix} \begin{bmatrix} \overrightarrow{T}_c \\ \overrightarrow{T}_w \\ \overrightarrow{T}_z \end{bmatrix} \\
&+ \begin{bmatrix} \widetilde{C}_c & 0 & 0 \\ 0 & \widetilde{C}_w & 0 \\ 0 & 0 & \widetilde{C}_{air} \end{bmatrix}^{-1} \widetilde{F} u
\end{aligned} \tag{4}$$

where $\widetilde{C}_c, \widetilde{C}_w,$ and $\widetilde{C}_{air}$ are the heat capacity matrix of the radiant ceiling, the other building envelopes, and the zone air. $\overrightarrow{T}_c, \overrightarrow{T}_w,$ and $\overrightarrow{T}_z$ are the temperature matrix of the radiant ceiling, the other building envelopes, and the zone air. $\widetilde{H}_c, \widetilde{H}_{cw},$ and $\widetilde{H}_{cz}$ are the conductive, radiant, and convective heat transfer coefficient matrix of

Table 1
Thermal performance parameters of the building envelope configurations of the experimental platform.

Envelope	Material	Heat transfer coefficient $W/m^2 \cdot K$	Specific heat capacity kJ/kg·K	Density kg/m^3	Thermal resistance $m^2 \cdot K/W$
Exterior wall	Solid brick wall (240 mm)	2.03	1.05	1500	0.492
Interior wall	Solid brick wall (180 mm)	2.39	1.05	1500	0.419
Floor	Precast concrete slabs	2.20	1.05	970	0.454
Window	Aluminum single glazed windows	6.40	/	/	0.156

the radiant ceiling which can be obtained after establishing the heat balance equation for every temperature node of the building envelopes. $\widetilde{H}_w$, $\widetilde{H}_{wc}$, and $\widetilde{H}_{wz}$are the conductive, radiant, and convective heat transfer coefficient matrix of the other building envelopes. $\widetilde{H}_{zc}$ is the convective heat transfer coefficient matrix between the radiant ceiling and the zone air while $\widetilde{H}_{zw}$ is the convective heat transfer coefficient matrix between the other building envelopes and the zone air and $\widetilde{H}_z$ is the convective heat transfer coefficient matrix of all the building envelope surfaces. $\vec{q}_c$ is the heat flow matrix of the radiant ceiling which includes the solar radiation on the radiant ceiling surface that is reflected from other internal surfaces and the heat supply from the water flow in the buried pipes. $\vec{q}_w$ refers to the convective and radiant heat flow matrix on the envelope surface while $\vec{q}_z$ is the convective heat flow matrix, such as the ventilation load and the infiltration load. F indicates the conversion form after separating the input variables such as water supply temperature, ambient temperature, and solar radiation, etc. from the heat flow matrix $\vec{q}_c$, $\vec{q}_w$, and $\vec{q}_z$. u refers to the input variables as mentioned previously. All these heat transfer matrices and the heat capacity matrix of the radiant ceiling cooling system are constructed with the thermal property parameters as shown in Table 1. The state-space representation of the radiant cooling ceiling system in Simulink is shown in Fig. 3.

Solar radiation is assumed to be distributed equally over all interior surfaces, including ceilings, floors, and envelope surfaces, as it is solar radiation is necessarily distributed over ceiling surfaces after multiple reflections from other surfaces, and is widely used in EnergyPlus and TRNSYS for appropriate simplification. However, this has no negative impact on the accuracy of the model. The ambient temperature is used to calculate the convective heat exchange on the outer surface of the enclosure, and the sky temperature is used to calculate the long-wave radiative heat exchange between the outer surface of the enclosure and the sky space. The combined effect of convective and radiative heat exchange on the enclosure surface is included in $\vec{q}_w$.

$R_{air-wall}$, $R_{air-ceiling}$, and $R_{air-floor}$ refer to the convective thermal resistors of the wall surfaces, the ceiling surface, and the floor surface, respectively of which, the convective thermal resistors on the internal and external envelope surfaces are assumed to be 0.115 $m^2 \cdot K/W$ and 0.043 $m^2 \cdot K/W$ and the convective thermal resistor on the internal ceiling surface is assumed to be 0.333 $m^2 \cdot K/W$ (3.0 $W/m^2 \cdot K$) on which there are comprehensive researches for refer-

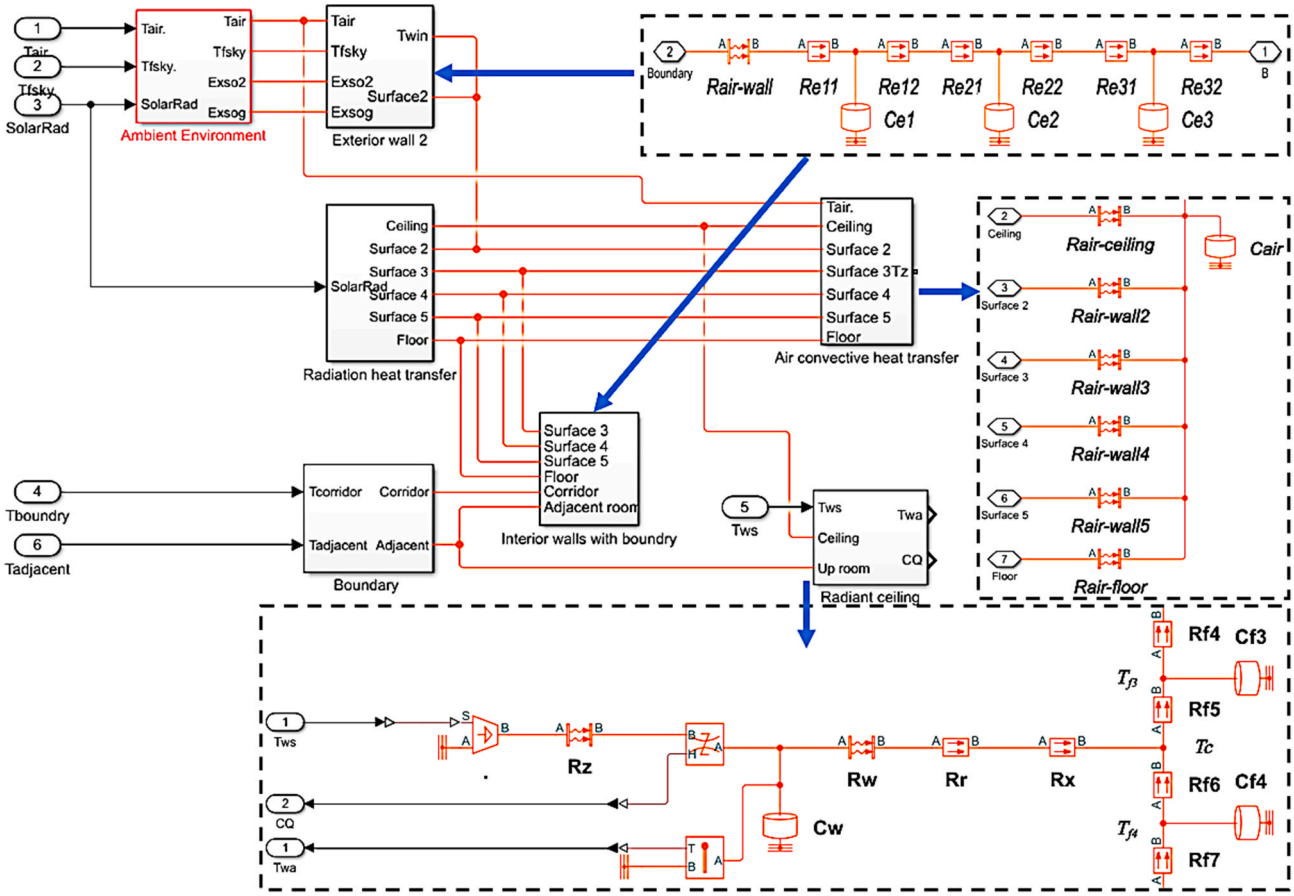

Fig. 3. The state-space representation of the radiant cooling ceiling system in Simulink.

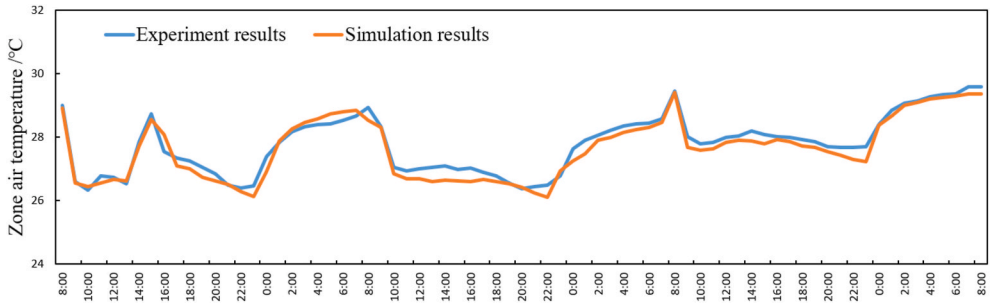

Fig. 4. The zone air temperatures results of the experiment and simulation results of the radiant ceiling cooling system.

ence [45]. The other R represents the conductive heat transfer coefficients of envelope layers. For a single material layer, the thermal resistor is calculated as $R = \delta/\lambda$, where δ indicates material layer thickness, (m). λ indicates the thermal conductivity of the material layer, $(W/m \cdot K)$. Thermal capacity is calculated as $C = c \cdot \rho \cdot V$, where c refers to the specific heat capacity of the material layer, $J/(kg \cdot ^\circ C)$ and ρ denotes the density of the material layer, (kg/m^3). R_z, R_w, R_r, and R_x denotes the thermal resistors between the water supply and return temperatures, the convective thermal resistor on the internal buried pipe surface, the conductive thermal resistor of the buried pipe, and the conductive thermal resistor of the core layer of the radiant ceiling, respectively. c represents the specific heat capacity of the envelope layers or the zone air. The radiant thermal resistors are calculated by the net radiosity method [46].

2.2. Building model validation

The MPC solves an open-loop optimal control problem that is independent of the specific model, but the accuracy of the predictive model has an essential influence on its implementation performance. Therefore, the accuracy of the state-space representation of the radiant cooling ceiling system is supposed to be validated precisely before its application to the control optimization.

The radiant ceiling system was turned on for cooling between 8:00–23:00 h and the setpoint of the zone air temperature was 27 °C during this period. Influenced by the ambient environment, the system was turned off at other periods and the zone air temperature was gradually increased. There was no occupant in the experimental cell during the experimental period. The zone air temperature, the ceiling surface temperature, and the interior surface temperatures were measured and recorded in the experiments for demonstrating the accuracy of the radiant ceiling, other envelopes, and zone air models established in the previous section.

All these temperatures were measured with T-type thermocouples, which were laid on the radiant ceiling surface and other envelope surfaces in a five-point layout which means that the five points were equally spaced on the diagonals of the surface. The indoor air temperatures at the heights of 0.1 m, 0.7 m, 1.1 m, and 1.7 m were measured and the temperatures at the heights of 1.1 m was considered as the experimental zone air temperature which is the height of the head when the human body sits down. All surface temperatures were the average temperature of the five measurement points laid on the surface in a plum-shaped arrangement. The uncooled surface temperature was taken as the average temperatures of other internal surfaces except the ceiling. All the T-type thermocouples used in the experiments were calibrated by the constant temperature tank method and the measurement error was calculated to be within 2.73%, which could meet the accuracy requirements of the experimental testing.

The zone air temperatures of the experiment and the simulation results of the radiant ceiling cooling system are shown in Fig. 4. The experimental zone air temperature was in the range of $26^\circ C$–$30^\circ C$ during the three typical operation days. Overall the simulated value of the zone air temperature was consistent with the experimental value. However, there were few discrepancies between the two when the zone air temperature was experiencing an increase or decrease in the streaming as the cooling load of the experimental cell changed due to the variable ambient temperature and solar radiation. The small discrepancy between the experimental and the simulation results of the zone air temperature established the excellent accuracy of the state-space representation of the radiant ceiling cooling system.

The ceiling surface temperatures results of the experiment and simulation results of the radiant ceiling cooling system are shown in Fig. 5. The experimental ceiling surface temperature ranged from $19^\circ C$–$30^\circ C$ during the three typical operation days. The water supply temperature of the radiant ceiling was maintained above 16 °C and the radiant ceiling surface temperature was kept above 19°Cas this was the lower limit above the zone air dew point temperature for preventing condensation on the radiant ceiling surface. The simulated value of the ceiling surface temperature followed the same trends as the experimental value in general. The few discrepancies between the two were almost negligible during the steady-state and the dynamic-state operation of the radiant ceiling system. The ceiling surface temperatures rose rapidly when the radiant ceiling cooling system shut down at 23:00 h and they descended quickly as the system started running at 8:00 h. The

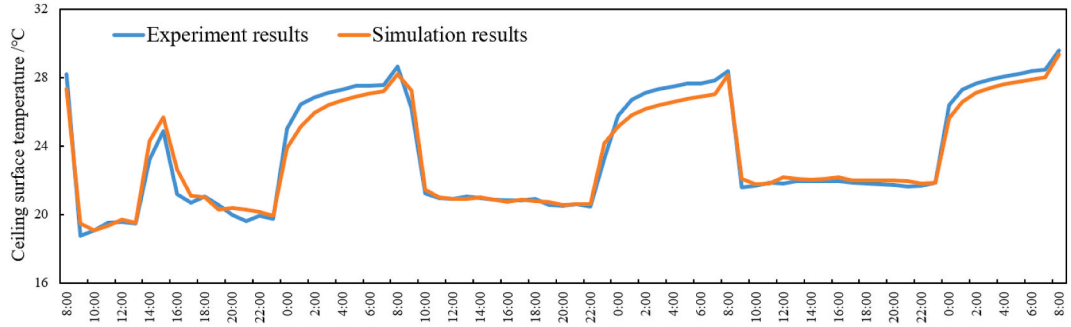

Fig. 5. The ceiling surface temperature results of the experiment and simulation results of the radiant ceiling cooling system.

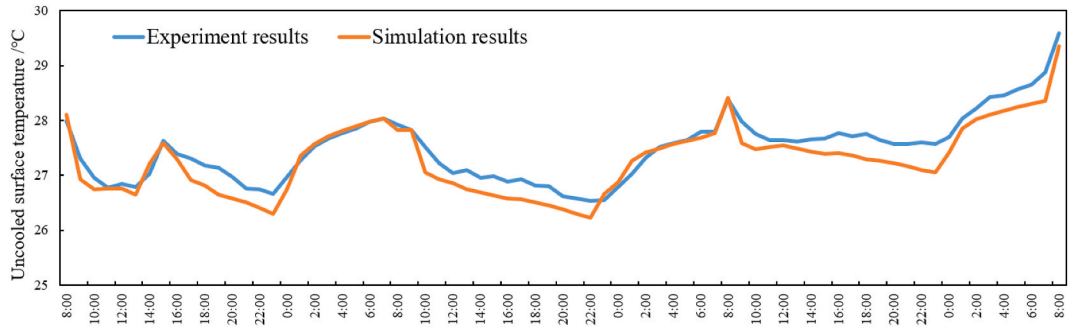

Fig. 6. The average uncooled surface temperature results of the experiment and simulation results of the radiant ceiling cooling system.

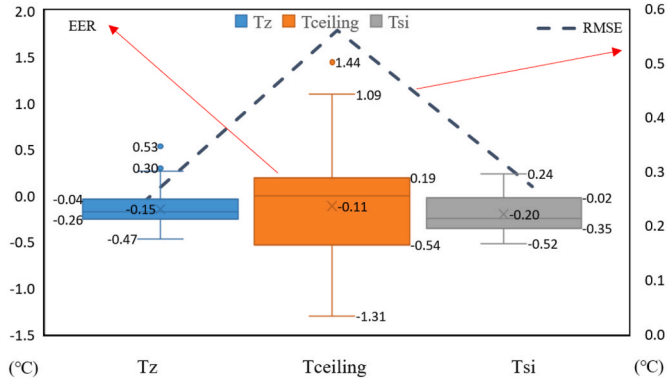

Fig. 7. The mean error (ERR) and root mean square error (RMSE) of the zone air temperature (T_z), the radiant ceiling surface temperature ($T_{ceiling}$), and the average uncooled surface temperature (T_{si}).

trends of the experimental and simulation results were almost identical in proving the excellent accuracy of the state-space model of the radiant ceiling.

The average uncooled surface temperature results of the experiment and the simulation of the radiant ceiling cooling system are shown in Fig. 6. The average uncooled surface temperature ranged from 26°*C*–30°*C* during the three typical operation days. The average uncooled surface temperatures fluctuated slower compared to that of the radiant ceiling surface temperature. It was influenced by the radiant heat exchange with the radiant ceiling and the convective heat exchange with the zone air, where there existed a certain delay and between the radiant ceiling and the uncooled interior surfaces. The simulated uncooled interior surface temperature was generally consistent with the experimental result, and its slightly larger error relative to the radiant ceiling surface resulted from that and was significantly influenced by more thermal disturbances such as infiltration load and boundary conditions. The few discrepancies of the experimental and simulation results demonstrated the excellent accuracy of the conductive, convective and radiant heat transfer model of the entire radiant ceiling system.

The mean error (ERR) and root mean square error (RMSE) of the zone air temperature (T_z), the radiant ceiling surface temperature ($T_{ceiling}$), and the average uncooled surface temperature (T_{si}) are shown in Fig. 7 and Table 2. The ERR of T_z, $T_{ceiling}$, and T_{si} were 0.15°*C*, 0.11°*C*, and 0.20°*C* on average, respectively while the RMSE of T_z, $T_{ceiling}$, and T_{si} were 0.24°*C*, 0.55°*C*, and 0.27°*C* on average, respectively. Both the ERR and RMSE of T_z, $T_{ceiling}$, and T_{si} were within the acceptable range for the practice application, establishing the excellent accuracy of the state-space model of the radiant ceiling cooling system.

3. Controller design

3.1. Model predictive control

The MPC, also known as the moving horizon control (MHC) or dynamic matrix control (DMC), is a state-of-the-art feedback control strategy that has been widely discussed and applied in recent years. The mechanism of MPC can be described as solving a finite time-domain open-loop optimization problem online during each sampling moment based on the current measurement information by applying the first element of the resulting control sequence to the control target. The process is repeated at the next sampling moment, i.e., the optimization problem is refined with online measurements and solved again. Solving the open-loop optimization problem online to obtain the control sequence is the main difference between the model predictive control and the traditional control methods since the latter usually outputs a feedback control sequence offline and applies all the control sequences to the system for one time. The MPC proposed in this research takes the uncertainty of thermal disturbances at an early stage of the algorithm design so that the optimized control system can still exhibit good stability in the face of large fluctuations of thermal disturbances.

The ambient temperature and solar radiation typically rise to the highest levels at midday when an increase in the building cooling load causes the zone air temperature to increase. If the water temperature of the ceiling radiant cooling system, which has high thermal inertia, is not reduced earlier to provide more cooling capacity to the thermal zone, it is likely to result in a significant overshoot of the zone air temperature.

Table 2
The mean error (ERR) and root mean square error (RMSE) of the zone air temperature (T_z), the radiant ceiling surface temperature ($T_{ceiling}$), and the average uncooled surface temperature (T_{si}).

Parameters	Zone air temperature (T_z)		Ceiling surface temperature (T_c)		Average uncooled surface temperature (T_{si})	
Error category	ERR (°C)	RMSE (°C)	ERR (°C)	RMSE (°C)	ERR (°C)	RMSE (°C)
Operation day 1	−0.03	0.23	−0.05	0.69	−0.13	0.23
Operation day 2	−0.23	0.28	−0.21	0.59	−0.16	0.24
Operation day 3	−0.18	0.21	−0.08	0.37	−0.30	0.33
Average error	−0.15	0.24	−0.11	0.55	−0.20	0.27

Notes. $\mathrm{ERR} = \sum_{k=0}^{N} (T_{simulation} - T_{experiment})/N.\mathrm{RMSE} = \sqrt{\sum_{k=0}^{N} (T_{simulation} - T_{experiment})^2/N}$

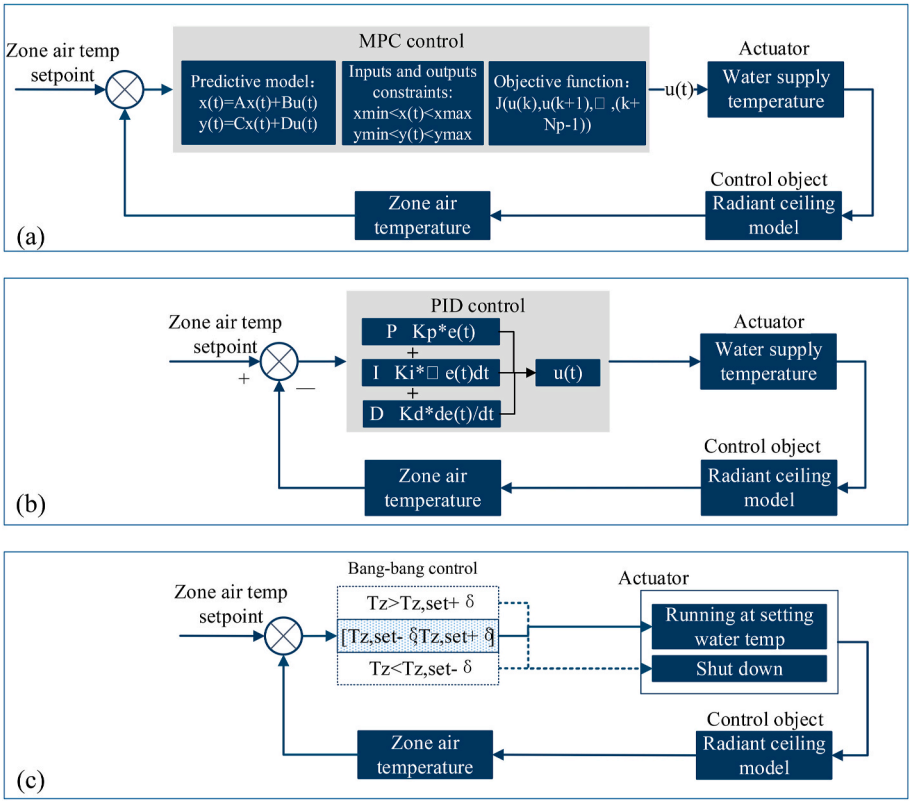

Fig. 8. The schematic diagram of the control scheme for MPC, PID control, and bang-bang control.

The control target of the zone air temperature will experience enormous fluctuations which demonstrates the robustness of the control system. In this study, the outdoor ambient temperature and solar radiation are considered as predictable disturbances that come from the weather forecast for the next day, which is proposed to improve the superior performance of the MPC for the radiant ceiling cooling system in maintaining stability against random thermal disturbance fluctuations.

$$\begin{cases} \dot{x}(t) = Ax(t) + Bu(t) + G\omega(t) \\ y(t) = Cx(t) + Du(t) + F\omega(t) \end{cases} \tag{5}$$

where $A \in R^{n*n}$, $B \in R^{n*p}, G \in R^{n*g}$, $C \in R^{q*n}$, $D \in R^{q*p}, F \in R^{q*g}$ refer to the coefficient matrix of the radiant ceiling cooling system which has been analyzed and addressed before based on the comprehensive heat transfer analysis of the radiant ceiling, other building envelopes, and the zone air. $x(t) \in R^{n}$, $u(t) \in R^{p}$, $\omega(t) \in R^{g}$, $y(t) \in R^{q}$ denote the temperature states vector, the input state vector of the supply water temperature, the thermal disturbances vector, including ambient temperature and solar radiation, and the output variables vector, such as the temperature and heat flux on the building surfaces.

The minimum value of the objective function is solved to obtain the optimal control sequence based on updating the real-time values of the thermal disturbances within each prediction time domain, while the control object of the zone air temperature tracks the reference trajectory as much as possible to prevent its large overshoot. According to the extensive analysis of simulation results, the prediction horizon is Np = 30, and the control horizon is Nc = 1. since a larger prediction horizon will lead to an enormous computational effort and a larger control horizon will cause the declining robustness performance of the MPC. A larger prediction range will lead to a significant increase in computational cost and a decrease in the control performance of the MPC. When the prediction range is chosen to be 30, the MPC is not too computationally intensive leading to the slower response of the control system, and nor is it not too small, leading to reduced robustness due to the insufficient consideration of thermal disturbances in the future. A variety of scenarios including different prediction horizons and control horizons have been compared in terms of the zone air temperature control, computational time, and energy consumption. The prediction horizon of 30 and control horizon of one is the optimal selection for the radiant ceiling system in this research.

$$\min\ J\left(u(k), u(k+1), \ldots, (k+N_p-1)\right) = \sum_{i=1}^{N_p} \left[\alpha(i)\left(T_{z,set}(k+i) - T_z(k+i)\right)^2 + r(i)\left((u(k+i) - u(k+i-1))/T_s\right)^2\right] \tag{6}$$

Constraint: $u_{min} \le u(k+i-1) \le u_{max}$

Where $T_z(k+i)$ refers to the predictive zone air temperature in the prediction horizon and $T_{z,set}(k+i)$ refers to the zone air temperature setpoint. $u(k+i)$ denotes the manipulated variables of the water supply temperature. $\alpha(i)$ and $r(i)$ denote the manipulated weights for the zone air temperature tracking and the water supply temperature variation restriction. And T_s refers to the sampling time taken as 300 s while u_{min} and u_{max} denotes the upper and lower limitations of the water supply temperatures, taken as 16°C and 30°C for preventing the condensation on the ceiling surface. The schematic diagram of the control scheme for the MPC is presented in Fig. 8 (a).

3.2. PID control

The PID control is designed and formulated for a comprehensive comparison with the dynamic characteristic performance with the MPC controller for accounting for about 90% of its applications in a wide variety of control systems. It is a kind of offline controller, of which the parameters are pre-set and will not be adjusted online as the system performance dynamically changes. It is particularly suitable for situations with little information about the target model. In this research, the water supply temperature was taken as the control variable and the zone

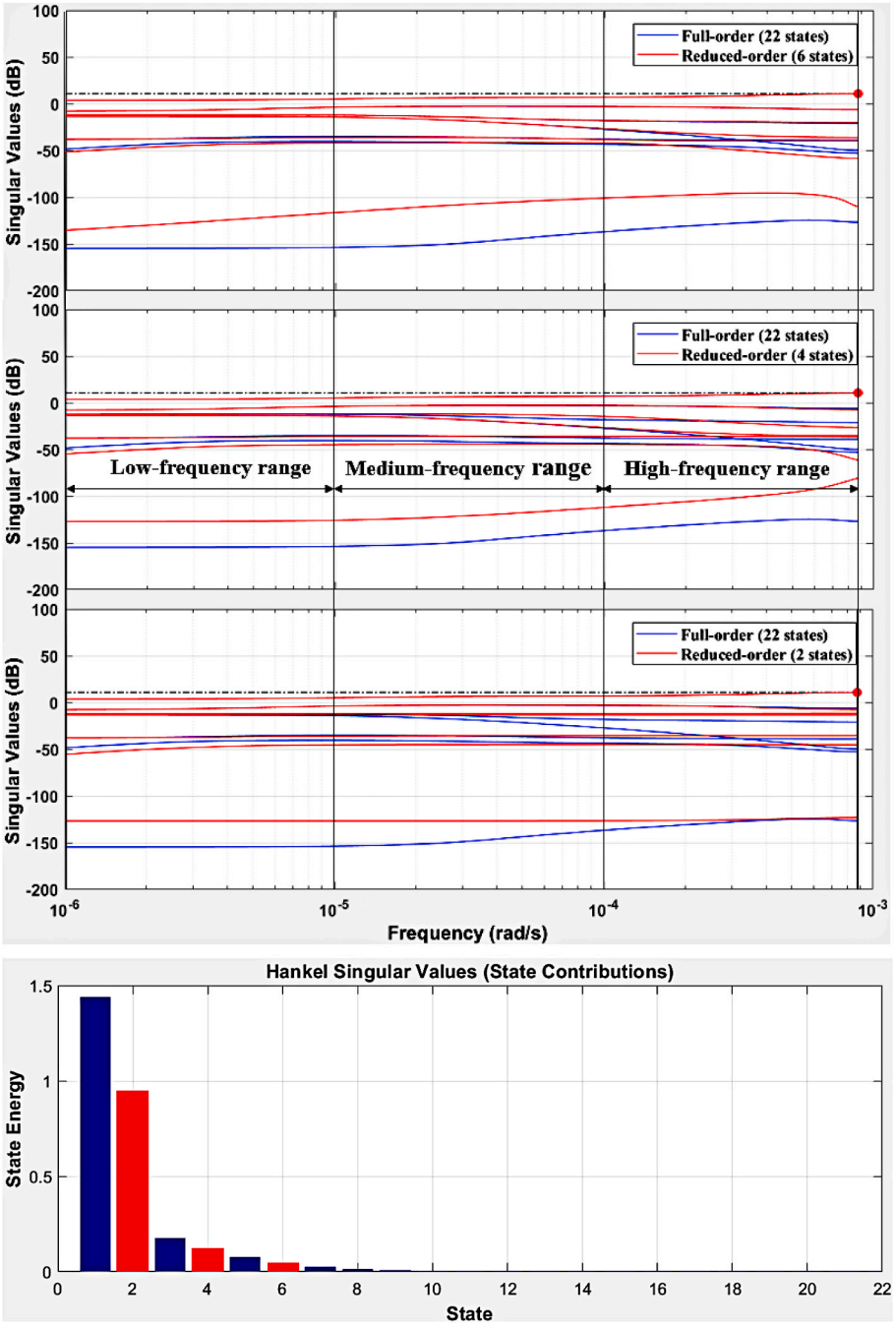

Fig. 9. Frequency domain response bode plots and Hankel singular values (HSVs) for the six-order model, the four-order model, and the two-order model.

air temperature was adopted as the objective variable for the PID control. The control sequences derived from the PID algorithm are demonstrated in Eq. (7).

$$u_k = K_p\left\{T_{z,k} + \frac{T}{T_i}\sum_{j=0}^{k} T_{z,j} + \frac{T_d}{T}\left(T_{z,k} - T_{z,k-1}\right)\right\} \tag{7}$$

where u_k refers to the water supply temperature which is required to be higher than $16°C$ for preventing the condensation on the ceiling surface. $T_{z,k}$ and $T_{z,k-1}$ refer to the zone air temperature at the current moment and the last moment, respectively while K_p, T_i, and T_d refer to the proportional gain, the integral time constant, and the differential time constant, respectively, which depend on the dynamic performance of the control target. T denotes the sampling time. In this research, K_p, T_i, and T_d are taken as 10, 0.02, and 10. The PID parameters were estimated by Ziegler Nichols at first, then the step response of the estimated PID control was further tested in the MATLAB Simulink environment. These parameters were finally selected after slightly tuning in MATLAB while the dynamic performance indicated by factors such as the rise time, settling time, and overshoot, etc. was evaluated. The schematic diagram of the control scheme for PID control is displayed in Fig. 8 (b).

3.3. Bang-bang control

Bang-bang control, as the simplest control strategy, is also widely used in air conditioning systems for residential buildings due to its advantages, such as easy installation and commissioning. The traditional

bang-bang control outputs only two states of control signals, either 'on' with a fixed constant or 'off' with a zero control signal. However, it is not sufficient for the traditional bang-bang control to meet the requirements of further improving the control accuracy and energy saving efficiency. The schematic diagram of the control scheme for the bang-bang control is exhibited in Fig. 8 (c). $T_{z,set}$ refers to the zone air temperature setpoint and δ denotes the dead band of the thermostat, which is normally counted as $0.5°C$ normally. The radiant ceiling cooling is running under the constant water supply temperature when the zone air temperature is set at the range of $T_{z,set} - \delta$ to $T_{z,set} + \delta$, which means that the system is shut down while the zone air temperature is lower than $T_{z,set} - \delta$. It is turned on again while the zone air temperature is higher than $T_{z,set} + \delta$.

4. Model order reduction

The MPC places high demands on the computational cost of the predictive model although the state-space model of the radiant ceiling system can meet the accuracy requirements. This is a very important factor affecting the dynamic performance of the MPC. Complex higher-order models can lead to a surge in the computation cost required for the MPC at each prediction step, which increases the CPU load on the computer while compromising the fast response characteristics of the MPC. Model order reduction techniques, which originated in the field of automatic control systems and circuit systems, have been successfully applied in the field of building heat transfer and humidity modeling as long as these techniques can reduce the model dimensionality while maintaining the accurate dynamic characteristics of the original system. Currently, the widely used model order reduction techniques include the proper orthogonal decomposition (POD), the Krylov subspace method, and the balanced truncation method. In this study, the balanced truncation method which has a wider range of applications in the field of building modeling is applied to truncate the redundant states of the original state-space model of the radiant ceiling system to obtain a simplified model that meets the requirements of in terms of accuracy as well as that of the computational effort.

The main concept of model order reduction is to truncate and remove the states in the higher-order model that contribute little to the system output, where the contribution of these states is judged based on the analysis of the controllability and observability of the model. In the practical application of radiant ceiling cooling systems, some of the temperature states in the original model are unobservable and uncontrollable, and the presence of these temperature states has an almost negligible impact on the model output. The dynamic characteristics of the original model can be retained while the model complexity and controller design can be simplified by truncating these unobservable and uncontrollable states. The computational effort of the MPC can be effectively reduced and has a considerable impact on its efficient application of MPC.

The balanced truncation method is a reduced-order method based on singular value decomposition which can yield a high-fidelity simplified model by a reasonable choice of mapping subspaces. First, the system model as shown in Eq. (8) is subjected to a state transition, i.e., the diagonalization of the Gramian matrix is implemented so that the uncontrollable states are transformed as the unobservable states simultaneously. The controllability Gramian and the observability Gramian are shown in Eq. (10) and Eq. (11).

$$\begin{cases} \dot{x}(t) = Ax(t) + Bu(t) \\ y(t) = Cx(t) + Du(t) \end{cases} \tag{8}$$

$$\Gamma(t) = \int_0^\infty Ce^{A(t+\tau)}B\vartheta(t)d\tau \tag{9}$$

Table 3
The mean error (ERR) and root mean square error (RMSE) of the zone air temperature (T_z), the radiant ceiling surface temperature ($T_{ceiling}$), and the average uncooled surface temperature (T_{si}) of the reduced-order models.

Parameters	Error	Six-order model	Four-order model	Two-order model
T_z	ERR (°C)	0.0004	0.0011	0.0002
	RMSE (°C)	0.0008	0.0152	0.0221
$T_{ceiling}$	ERR (°C)	0.0012	0.0006	0.0022
	RMSE (°C)	0.0032	0.0155	0.0468
T_{si}	ERR (°C)	0.0001	−0.0010	−0.0007
	RMSE (°C)	0.0005	0.0028	0.0060

Notes. ERR $= \sum_{k=0}^{N} (T_{reduced-order} - T_{full-order})/N$

$$W_c = \int_0^\infty e^{A\tau}BB^T e^{A^T\tau}d\tau \tag{10}$$

$$W_O = \int_0^\infty e^{A^T\tau}C^T Ce^{A\tau}d\tau \tag{11}$$

where $x(t) \in R^n$ denotes the state matrix of the n temperature states in the building model at moment t, $u(t) \in R^p$ denotes the input vector at moment t, such as ambient temperature, solar radiation, and water supply temperature, etc. $y(t) \in R^q$ denotes the output vector of the building model at moment t, such as the zone air temperature and surface temperatures. $A \in R^{n*n}$, $B \in R^{n*p}$ $C \in R^{q*n}$, $D \in R^{q*p}$ are the coefficients matrices representing the relationship between the inputs and outputs of the state-space model of the radiant ceiling system.

The importance of the states can be measured by the singular values of the Hankel operator in Eq. (9). In other words, the contribution of each state to the model output can be determined if the Hankel singular value (HSV) expressed by $\sum$ can be found. The HSV is solved by the formula $W_O = W_c = \sum$. Then the Galerkin projection of the original model is constructed based on the HSVs, and the reduced-order model, as shown in Eq. (12), obtained by applying the balanced truncation method can maintain most of the dynamic characteristics of the original model.

$$\begin{cases} \dot{\check{x}}(t) = \check{A}\check{x}(t) + \check{B}u(t) \\ \check{y}(t) = \check{C}\check{x}(t) + \check{D}u(t) \end{cases} \tag{12}$$

The reduced-order models with the different number of states were obtained after truncating the uncontrollable and unobservable states of the original model of the radiant ceiling system with 22 orders (including 22 temperature states). The frequency-domain response bode plots for the six-order model, the four-order model, and the two-order model is shown in Fig. 9. The frequency-domain response bode plots of the six-order model and the original-order model overlapped almost similarly, whether they were in the high, middle, or low-frequency regions. The frequency-domain response of most of the outputs of the four-order model matched very well with that of the original-order model, with only a minor discrepancy in some of the outputs. As the order was further reduced, some of the outputs of the two-order model differ more significantly from the original-order model in the middle and low-frequency regions, as can be seen by the larger discrepancy between the blue solid line and the red solid line in the figure.

HSVs of the six-order model, the four-order model, and the two-order model are shown in Fig. 9. The HSVs gradually increased from 0 to about 1.5 as the order of the models decreased. The HSVs of the reduced-order models were higher than 0 while that of the reduced-order model were less than nine orders (1–8 orders). Then the important orders that have made a greater contribution to the original model accuracy will be

Table 4
Comparison of computational time for the open-loop simulation for the six-order model, the four-order model, and the two-order model.

Step size	5 min		10 min		30 min	
Simulation durations	30 days	365 days	30 days	365 days	30 days	365 days
Full-order model (s)	0.763	0.979	0.754	0.968	0.743	0.909
Six-order model (s)	0.655	0.793	0.634	0.792	0.728	0.770
Four-order model (s)	0.631	0.725	0.622	0.716	0.607	0.712
Two-order model (s)	0.580	0.641	0.558	0.572	0.507	0.541
Max relative ratio (%)	−24.0%	−34.5%	−26.0%	−40.9%	−31.8%	−40.5%

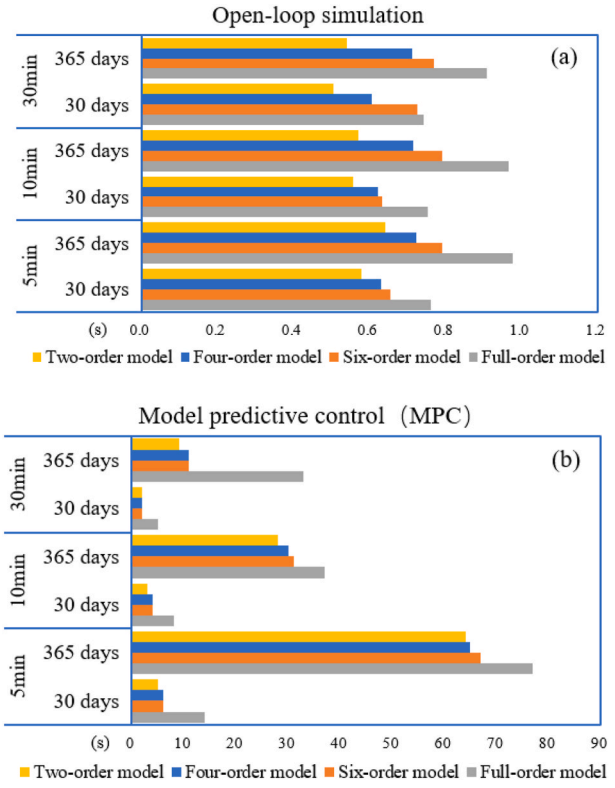

Fig. 10. Comparison of computational time for the open-loop simulation and model predictive control for the six-order model, the four-order model, and the two-order model for the radiant ceiling system.

truncated. Therefore, the reduced-order model with more than nine orders can keep the full dynamic performance of the original model. Therefore, the accuracy and computational effort of the six-order model, the four-order model, and the two-order model were analyzed separately below.

The ERR and RMSE of the zone air temperature (T_z), the radiant ceiling surface temperature ($T_{ceiling}$), and the average uncooled surface temperature (T_{si}) of the reduced-order models are exhibited in Table 3. For the six-order model, the ERR of T_z, $T_{ceiling}$, and T_{si} were $0.0004°C$, $0.0012°C$, and $0.0001°C$ on average, respectively. The RMSE of T_z, $T_{ceiling}$, *and* T_{si} were $0.0008°C$, $0.0032°C$, and $0.0005°C$ on average, respectively. The errors of T_z, $T_{ceiling}$, and T_{si} for the four-

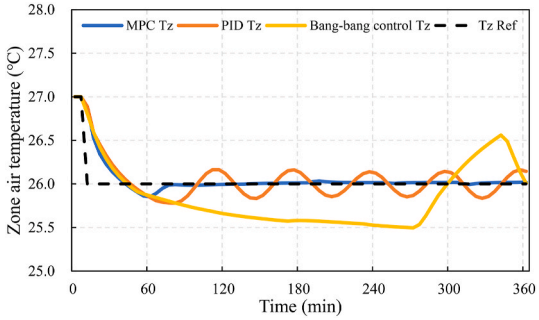

Fig. 11. The zone air temperature responses for MPC, PID control, and bang-bang control.

order and two-order models were still relatively lower literally although their RMSE was slightly larger than that of the six-order model, which can be explained synthetically by the relatively lower HVS of the six-order model. The extremely small order of the magnitude of ERR and RMSE of T_z, $T_{ceiling}$, and T_{si} can confirm the remarkable accuracy of the reduced-order model of the radiant ceiling cooling system.

$$RMSE = \sqrt{\sum_{k=0}^{N} \left(T_{reduced-order} - T_{full-order}\right)^2 / N}$$

Table 4 and Fig. 10 (a) show the comparison of computational time for the open-loop simulation for the six-order model, the four-order model, and the two-order model when the simulation steps are 5 min, 10 min, and 30 min, and the simulation durations are 30 days and 365 days, respectively. The computation time for the six-order model, the four-order model, and the two-order model ranged from 0.634–0.793 s, 0.607–0.725 s, and 0.507–0.641 s, while that of the full-order model was 0.743–0.979 s. The computational efficiency was improved by 24.0%–40.9%.

Comparison of computational time of the MPC for the six-order model, the four-order model, and the two-order model was shown in Table 5 and Fig. 10 (b). The computation time of the MPC system was much larger than that of the open-loop simulation. The computation time for the six-order model, the four-order model, and the two-order model ranged from 2–67 s, 2–65 s, and 2–64 s, respectively, while that of the full-order model was 5–77 s. The computational efficiency was improved by 16.9%–72.7%. The balanced truncation method effectively reduces the model complexity, and the resulting boost in the computational efficiency of the MPC system is highly promising, while

Table 5
Comparison of computational time of model predictive control (MPC) for the six-order model, the four-order model, and the two-order model.

Step size	5 min		10 min		30 min	
Simulation durations	30 days	365 days	30 days	365 days	30 days	365 days
Full-order model (s)	14	77	8	37	5	33
Six-order model (s)	6	67	4	31	2	11
Four-order model (s)	6	65	4	30	2	11
Two-order model (s)	5	64	3	28	2	9
Max relative ratio (%)	−64.3%	−16.9%	−62.5%	−24.3%	−60.0%	−72.7%

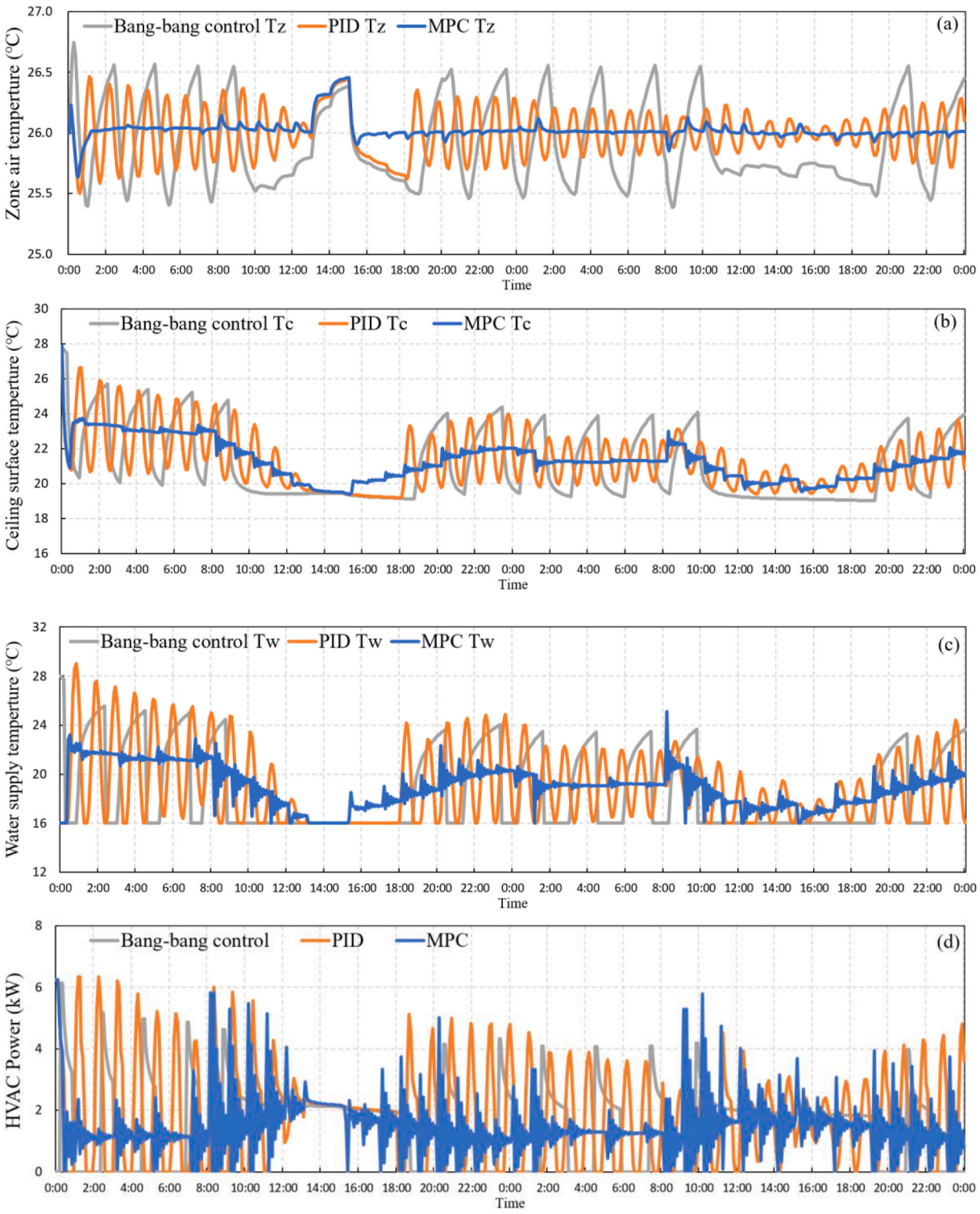

Fig. 12. The zone air temperature, the ceiling surface temperature, the water supply temperature, and HVAC power for MPC, PID control, and bang-bang control under continuous operation.

the potential advantages of the model reduction technique in the simplification of large-scale building models are more extensive.

5. Results and discussion

The zone air temperature responses for the MPC, PID control, and bang-bang control are shown in Fig. 11. It was seen that the offset band between setpoint temperature and the zone air temperature was negligible for the MPC, while it was 0.2°*C* and 0.6°*C* for the PID control and the bang-bang control, respectively. The response time of the zone air temperature was the same for the three control methods.

5.1. Continuous operation

The zone air, ceiling surface, and the water supply temperatures for the MPC, PID control, and bang-bang control under a continuous oper-

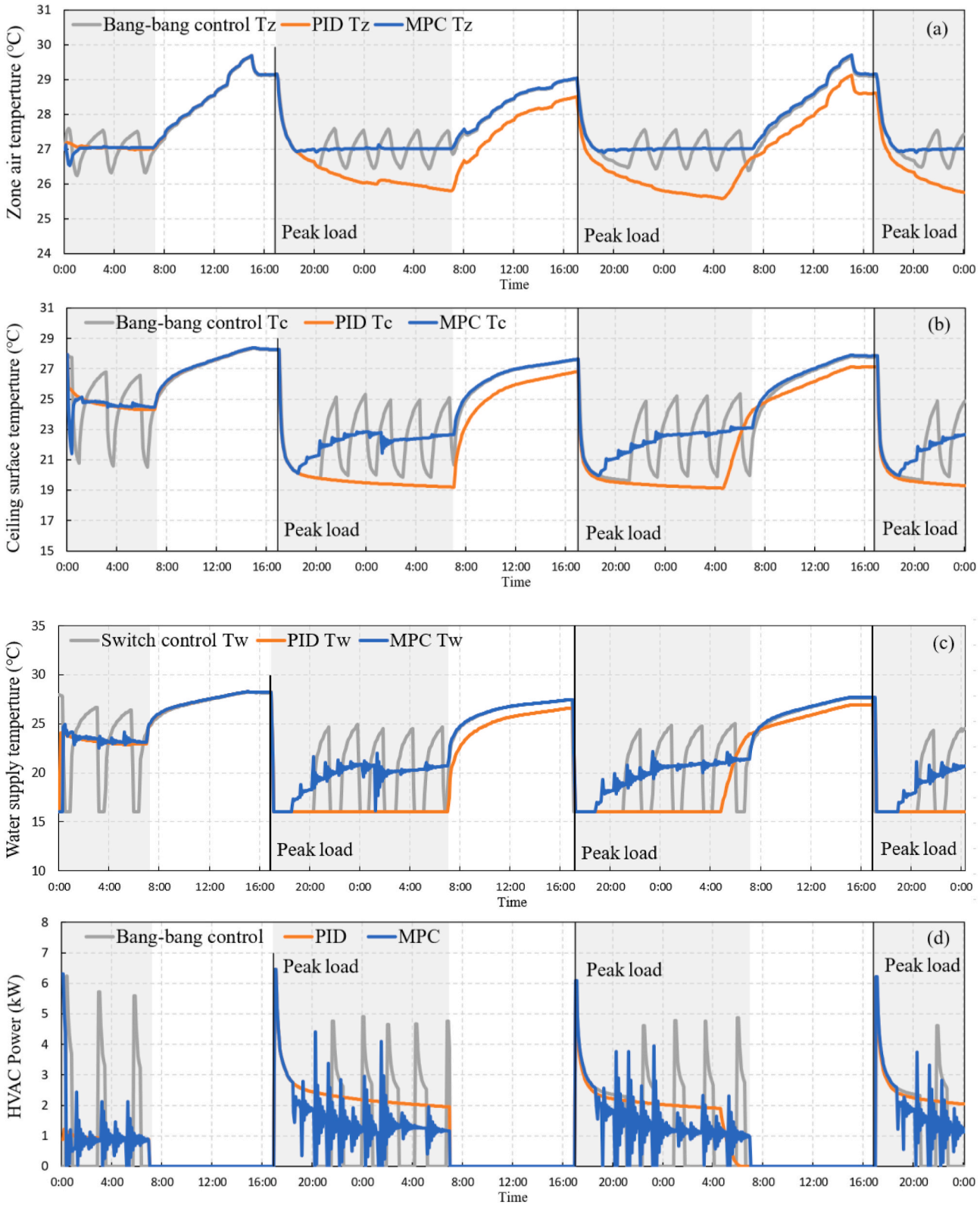

Fig. 13. The zone air temperature, the ceiling surface temperature, the water supply temperature, and HVAC power for the MPC, PID control, and bang-bang control under intermittent operation.

ation are presented in Fig. 12. The zone air temperature of the MPC was stable at the setpoint firmly for the operation duration with only a 0.4°*C* offset band variation at 14:00 h for the first 24 h due to the sharp increase of the solar radiation and cooling load of the buildings. The zone air temperature of the PID control experienced an 0.1°*C*–0.4°*C* offset band variation from the setpoint while there was about a 0.6°*C* offset band variation from the setpoint for the bang-bang control.

The ceiling surface temperatures were above 19°*C* for preventing the consideration on the radiant ceiling surface under the three controllers' operation. The ceiling surface temperature of the MPC varied slowly

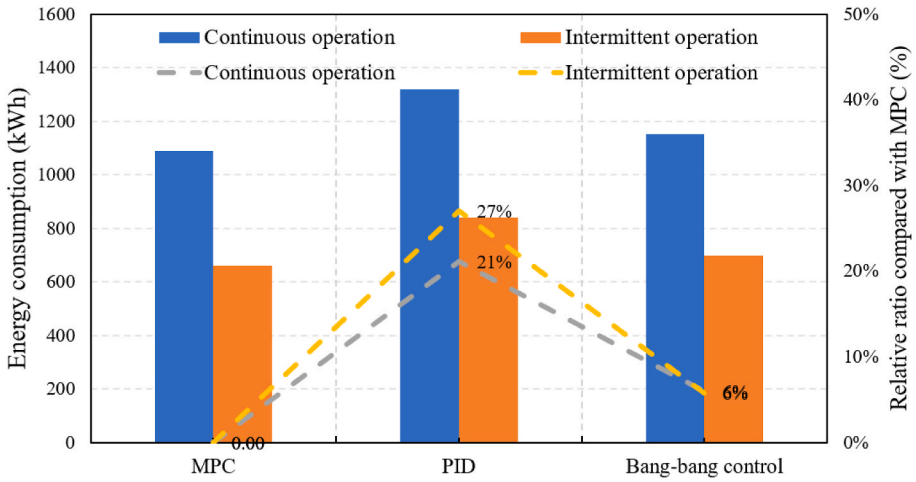

Fig. 14. The energy consumption under the continuous and intermittent operation for MPC, PID control, and bang-bang control and the relative ratio comparison.

within 19°*C*–23°*C* while that of the PID control and the bang-bang control experienced more frequent oscillations similar to the zone air temperature variation trends.

The water supply temperatures for the three controllers were above 16°*C* to avoid condensation on the radiant ceiling surface, which explained the 0.4°*C* offset band of the zone air temperature for the MPC since a lower water temperature cannot be available. The water supply temperature ranged from 16°*C*–22°*C* for the MPC. The water supply temperatures for the PID control and the bang-bang control ranged from 16°*C*–28°*C*. The water supply temperature of the MPC and the PID control fluctuated more frequently than that of the bang-bang control.

The HVAC power of the MPC that refers to the power consumption of the chiller increased to 6 kW at the maximum as the building cooling load increased and the water temperature decreased. The water supply temperature maintained a higher level which met the requirements of the zone air temperature tracking while the building cooling load decreased, as the HVAC power decreased to 1 kW–3 kW. The HVAC power of the radiant ceiling cooling system was kept within 4 kW–6 kW for most of the continuous operation's duration.

For radiant ceiling cooling systems, the MPC offers better performance in terms of zone air temperature control and energy-saving efficiency because it can adjust the water temperature in real-time as outdoor thermal disturbances and building cooling loads change. On the other hand, the model-free control, such as PID control and bang-bang control, is generally designed for a single operating condition, and the control system is less adaptive to external thermal disturbances.

5.2. *Intermittent operation*

In this section, the dynamic performance of the MPC, PID control, and bang-bang control under the intermittent operation of radiant ceiling cooling systems is analyzed. The system is shut down during the period from 8:00–18:00 h and is turned on during the other periods of the day.

Under the intermittent operation, the peak load of the radiant ceiling cooling system during the initial time under intermittent operation was very large, and a water supply temperature higher than 16°*C* was required for anti-condensation. This results in the limited cooling capacity of the radiant ceiling cooling system. Therefore, the zone air temperature under the intermittent operation was set to 27°*C* since the fan coil unit system is usually added to make up for the lack of efficient cooling capacity of the radiant ceiling system in practice.

The zone air, ceiling surface, and the water supply temperatures for the MPC, PID control, and bang-bang control under intermittent operation are presented in Fig. 13. The zone air temperature of the MPC was also firmly stable at the setpoint for the entirety of the operation duration without any overshoot. At the maximum, there was a 1.2°*C* of overshoot of the zone air temperature for PID control under an intermittent operation. The zone air temperature for bang-bang control was around the band of 26.5°*C*–27.5°*C* after reaching the setpoint.

The ceiling surface temperature for the MPC dropped to a minimum of 20°*C* during the peak load phase, after which the water temperature slowly rose back to a maximum of 23°*C* during the system stabilization phase. The ceiling surface temperature for the PID control dropped rapidly to about 20°*C* during the peak load phase, and thereafter further descended at a relatively slow rate to about 19°*C*. The ceiling surface temperature for bang-bang control oscillated continuously between 20°*C* and 25°*C* depending on the zone air temperature fluctuations.

The water supply temperature for the MPC maintained the minimum water temperature of 16°*C* in the peak load stage after the 80-min operation and slowly rose to a maximum of about 21°*C*. The water temperature of the PID control designed for continuous operating conditions maintained a minimum value of 16°*C* under intermittent operation conditions, which was the reason for the significant overshoot of the zone air temperature of 1.2°*C*. The water temperature was kept at 16°*C* for 3 h during the peak load phase and then fluctuated in the range of 16°*C*–25°*C*.

Unfortunately, when applied to the various other operation conditions, the PID controller failed to regulate the zone air temperature under the intermittent operation due to the poor adaption capacity of the designed PID controller for certain scenarios. The designed PID controller for the continuous operation cannot bear the cooling load surge at the initial moment under an intermittent operation. Besides, if the PID controller is designed for the intermittent operation, it will lead to a greater zone air temperature overshoot under the continuous operation, which has been evaluated by a simulation before. This is also the common disadvantage of the conventional PID controller compared with all kinds of adaptive and robust control methods.

During the peak load phase, the HVAC power of the three control methods reached a maximum of about 6 kW. The MPC had an average power of about 1.5 kW during the stable operation phase, while the PID control had the next highest power of about 2.2 kW and the bang-bang control had a maximum power of about 5 kW.

According to the simulation results under continuous and intermittent operation conditions, the MPC had the best robustness for the dynamic control of the radiant ceiling cooling system. The zone air temperature could be almost completely stabilized at the set value, and the water temperature could change smoothly and be kept as high as possible, which was beneficial to the energy saving operation of the system.

The energy consumption under the continuous and intermittent operation for the MPC, PID control, and bang-bang control and the

relative ratio comparison are shown in Fig. 14. The PID control increased energy consumption by 21% for continuous operation and about 27% for intermittent operation compared to the MPC for the radiant ceiling cooling system, while the bang-bang control increased energy consumption by about 6% for both continuous and intermittent operation compared to the MPC, which confirmed that the latter is more energy-efficient compared with conventional PID control and the bang-bang control for the radiant ceiling cooling system.

6. Conclusion

In this research, the state-of-the-art model predictive control for the radiant ceiling cooling system was proposed for zone air temperature tracking and energy efficiency. It was seen that it was more adaptive to the external thermal disturbances obtained such as solar radiation and ambient temperature. The physics-based model was developed based on the material property and geometric dimensions of building envelopes. Then the reduced-order model of the radiant ceiling cooling system was then obtained using the balanced truncation method for a lower computational cost while maintaining the model accuracy. Compared with PID control and conventional bang-bang control, the advanced performance of the proposed MPC in terms of an accurate zone air temperature tracking and energy efficiency was evaluated by a simulation under continuous and intermittent operations. The simulation results showed that the proposed MPC can achieve 21%–27% and 6% energy saving efficiency, compared with conventional PID control and bang-bang control, respectively, for the radiant ceiling cooling system, respectively. There was rarely any overshoot or steady-state error presence for the zone air temperature, which demonstrated the significant potential of applying the MPC to achieve the improved zone air temperature control and energy-saving efficiency for radiant ceiling cooling systems.

Declaration of competing interest

The authors declare that they have no known competing financial interests or personal relationships that could have appeared to influence the work reported in this paper.

References

[1] D. Kim, J.E. Braun, Model predictive control for supervising multiple rooftop unit economizers to fully leverage free cooling energy resource [J], Appl. Energy 275 (2020), 115324.

[2] Y. Yao, D.K. Shekhar, State of the art review on model predictive control (MPC) in Heating Ventilation and Air-conditioning (HVAC) field [J], Build. Environ. 200 (2021), 107952.

[3] S. Freund, G. Schmitz, Implementation of model predictive control in a large-sized, low-energy office building [J], Build. Environ. 197 (2021), 107830.

[4] F. Zhang, H.-A. Guo, Z. Liu, et al., A critical review of the research about radiant cooling systems in China [J], Energy Build. 235 (2021), 110756.

[5] M. Bai, F. Wang, J. Liu, et al., Experimental and numerical studies of heat and mass transfer performance and design optimization of Fan-coil with high supply chilled water temperature in Air-Conditioning system [J], Sustainable Energy Technologies and Assessments 45 (2021), 101209.

[6] G. Shen, Z.E. Lee, A. Amadeh, et al., A data-driven electric water heater scheduling and control system [J], Energy Build. 242 (2021), 110924.

[7] J. Wang, S. Li, H. Chen, et al., Data-driven model predictive control for building climate control: three case studies on different buildings [J], Build. Environ. 160 (2019), 106204.

[8] J. Feng, F. Bauman, Critical review of water based radiant cooling system design methods [J], Indoor Air 2014 - 13th International Conference on Indoor Air Quality and Climate (2014) 337–344.

[9] M.A. Hassan, O. Abdelaziz, Best practices and recent advances in hydronic radiant cooling systems – Part II: simulation, control, and integration [J], Energy Build. 224 (2020), 110263.

[10] J. Joe, P. Karava, A model predictive control strategy to optimize the performance of radiant floor heating and cooling systems in office buildings [J], Appl. Energy 245 (2019) 65–77.

[11] M. KRAJČÍK, O. Šikula, Heat storage efficiency and effective thermal output: indicators of thermal response and output of radiant heating and cooling systems [J], Energy Build. 229 (2020), 110524.

[12] X. Pang, C. Duarte, P. Haves, et al., Testing and demonstration of model predictive control applied to a radiant slab cooling system in a building test facility [J], Energy Build. 172 (2018) 432–441.

[13] A. Ghahramani, K. Zhang, K. Dutta, et al., Energy savings from temperature setpoints and deadband: quantifying the influence of building and system properties on savings [J], Appl. Energy 165 (2016) 930–942.

[14] Z. Wu, N. Li, P. Wargocki, et al., Field study on thermal comfort and energy saving potential in 11 split air-conditioned office buildings in Changsha, China [J], Energy 182 (2019) 471–482.

[15] M. Ławryńczuk, P. Ocioń, Model Predictive Control and energy optimisation in residential building with electric underfloor heating system [J], Energy 182 (2019) 1028–1044.

[16] X. Li, Z. Han, T. Zhao, et al., Modeling for indoor temperature prediction based on time-delay and Elman neural network in air conditioning system [J], Journal of Building Engineering 33 (2021), 101854.

[17] Z. Li, J. Zhang, Study on the distributed model predictive control for multi-zone buildings in personalized heating [J], Energy Build. 231 (2021), 110627.

[18] T. Shaqarin, A.E. Al-Rawajfeh, M.G. Hajaya, et al., Model-based robust H∞ control of a granulation process using Smith predictor with Reference updating [J], J. Process Contr. 77 (2019) 38–47.

[19] J. Drgoňa, J. Arroyo, I. Cupeiro Figueroa, et al., All you need to know about model predictive control for buildings [J], Annu. Rev. Contr. 50 (2020) 190–232.

[20] S. Yang, M.P. Wan, W. Chen, et al., An adaptive robust model predictive control for indoor climate optimization and uncertainties handling in buildings [J], Build. Environ. 163 (2019), 106326.

[21] M. Tesfay, F. Alsaleem, P. Arunasalam, et al., Adaptive-model predictive control of electronic expansion valves with adjustable setpoint for evaporator superheat minimization [J], Build. Environ. 133 (2018) 151–160.

[22] J. Drgoňa, D. Picard, L. Helsen, Cloud-based implementation of white-box model predictive control for a GEOTABS office building: a field test demonstration [J], J. Process Contr. 88 (2020) 63–77.

[23] N. Kayaci, Energy and exergy analysis and thermo-economic optimization of the ground source heat pump integrated with radiant wall panel and fan-coil unit with floor heating or radiator [J], Renew. Energy 160 (2020) 333–349.

[24] J. Fang, R. Ma, Y. Deng, Identification of the optimal control strategies for the energy-efficient ventilation under the model predictive control [J], Sustainable Cities and Society 53 (2020), 101908.

[25] J. Oravec, M. BAKOŠOVÁ, L. GALČÍKOVÁ, et al., Soft-constrained robust model predictive control of a plate heat exchanger: experimental analysis [J], Energy 180 (2019) 303–314.

[26] C. Zhang, M. Pomianowski, P.K. Heiselberg, et al., A review of integrated radiant heating/cooling with ventilation systems- Thermal comfort and indoor air quality [J], Energy Build. 223 (2020), 110094.

[27] C. Vallianos, A. Athienitis, J. Rao, Hybrid ventilation in an institutional building: modeling and predictive control [J], Build. Environ. 166 (2019), 106405.

[28] S. Yang, M.P. Wan, B.F. Ng, et al., Experimental study of a model predictive control system for active chilled beam (ACB) air-conditioning system [J], Energy Build. 203 (2019), 109451.

[29] S. Yuan, C. Vallianos, A. Athienitis, et al., A study of hybrid ventilation in an institutional building for predictive control [J], Build. Environ. 128 (2018) 1–11.

[30] D. Zhang, N. Cai, X. Cui, et al., Experimental investigation on model predictive control of radiant floor cooling combined with underfloor ventilation system [J], Energy 176 (2019) 23–33.

[31] D. Zhang, X. Huang, D. Gao, et al., Experimental study on control performance comparison between model predictive control and proportion-integral-derivative control for radiant ceiling cooling integrated with underfloor ventilation system [J], Appl. Therm. Eng. 143 (2018) 130–136.

[32] M.M. Mazar, A. Rezaeizadeh, Adaptive model predictive climate control of multi-unit buildings using weather forecast data [J], Journal of Building Engineering 32 (2020), 101449.

[33] S. Bella, A. Houari, A. Djerioui, et al., Robust Model Predictive Control (MPC) for large-scale PV plant based on paralleled three-phase inverters [J], Sol. Energy 202 (2020) 409–419.

[34] A. Buonomano, U. Montanaro, A. Palombo, et al., Temperature and humidity adaptive control in multi-enclosed thermal zones under unexpected external disturbances [J], Energy Build. 135 (2017) 263–285.

[35] S. Yang, M.P. Wan, B.F. Ng, et al., A state-space thermal model incorporating humidity and thermal comfort for model predictive control in buildings [J], Energy Build. 170 (2018) 25–39.

[36] I. Cupeiro Figueroa, D. Picard, L. Helsen, Short-term modeling of hybrid geothermal systems for Model Predictive Control [J], Energy Build. 215 (2020), 109884.

[37] T. Pippia, J. Lago, R. De Coninck, et al., Scenario-based nonlinear model predictive control for building heating systems [, J]. Energy and Buildings (2021), 111108.

[38] C. Ghiaus, N. Ahmad, Thermal circuits assembling and state-space extraction for modelling heat transfer in buildings [J], Energy 195 (2020), 117019.

[39] A. Afram, F. Janabi-Sharifi, Theory and applications of HVAC control systems – a review of model predictive control (MPC) [J], Build. Environ. 72 (2014) 343–355.

[40] A. Martinčević, M. Vašak, V. Lešić, Identification of a control-oriented energy model for a system of fan coil units [J], Contr. Eng. Pract. 91 (2019), 104100.

[41] T. Hoyt, E. Arens, H. Zhang, Extending air temperature setpoints: simulated energy savings and design considerations for new and retrofit buildings [J], Build. Environ. 88 (2015) 89–96.

[42] Q. Chen, N. Li, W. Feng, Model predictive control optimization for rapid response and energy efficiency based on the state-space model of a radiant floor heating system [J], Energy Build. 238 (2021), 110832.

[43] D. Kim, J.E. Braun, A general approach for generating reduced-order models for large multi-zone buildings [J], J Build Perf Simul 8 (2014) 435–448.
[44] M. Gwerder, J. TöDTLI, B. Lehmann, et al., Control of thermally activated building systems (TABS) in intermittent operation with pulse width modulation [J], Appl. Energy 86 (2009) 1606–1616.
[45] K.-N. Rhee, K.W. Kim, A 50 year review of basic and applied research in radiant heating and cooling systems for the built environment [J], Build. Environ. 91 (2015) 166–190.
[46] D. Kim, J.E. Braun, REDUCED-ORDER building modeling for application to model-based predictive control [J], Proceedings of SimBuild 8 (2012).